

# Cretaceous Vertical Motion of Australia and the Australian-Antarctic Discordance

Michael Gurnis, R. Dietmar Müller, Louis Moresi

A three-dimensional model of mantle convection in which the known history of plate tectonics is imposed predicts the anomalous Cretaceous vertical motion of Australia and the present-day distinctive geochemistry and geophysics of the Australian-Antarctic Discordance. The dynamic models infer that a subducted slab associated with the long-lived Gondwanaland-Pacific converging margin passed beneath Australia during the Cretaceous, partially stagnated in the mantle transition zone, and is presently being drawn up by the Southeast Indian Ridge.

Two perplexing features of plate tectonics are associated with the Australian plate (AUS): the complete subaerial exposure of Australia during the Cretaceous global sea-level maximum and the existence of a cold spot, possibly a convective downwelling, beneath the Australian-Antarctic spreading center. Stratigraphic and paleogeographic data demonstrate that broad regions of Australia underwent vertical motion without substantial folding or faulting during the Mesozoic and Cenozoic (1). Marine geophysical and geochemical evidence (2, 3) points toward a cold convective downwelling beneath the Southeast Indian Ridge (SEIR) at the position of the Australian-Antarctic Discordance (AAD), which is the deepest portion of the global mid-ocean ridge system. For the AAD, the regional mechanisms causing the low topography have been explored (4), but the more fundamental question as to why there is a cold spot, possibly a downwelling, beneath a spreading center has not been addressed. Aside from geologic correlations made by Veevers (5), the relation between these two features has not been determined.

During the Cretaceous, the marine inundation of Australia and the global (eustatic) sea-level curves were out of phase (Fig. 1). Maximum flooding of Australia occurred in the late Aptian to early Albian, 120 to 110 million years ago (Ma) (6), when large regions of the craton, especially in the east, and continental margins experienced marine inundation (Fig. 2A). Dur-

ing the Late Cretaceous, Australia became progressively exposed, with a flooding minimum in the Campanian, 80 to 70 Ma, when eustatic sea level was inferred to be near a maximum (1). These apparently incongruous relative sea-level curves support the hypothesis that Australia experienced several episodes of vertical motion, including a large-scale vertical translation of the entire continent and a localized subsidence event (1, 7, 8). During the Early Cretaceous, the vertical motion appears to have been confined to a smaller area in the east defined by the Eromanga and Surat basins (Fig. 2A, red outline) (9). Near the end of the Cretaceous, Australia was about 250 m higher than it is today (1, 7, 8). Some time during the Cenozoic, Australia appears to have subsided, perhaps with little tilting (8), as the continent moved northward after it separated from Antarctica.

Superimposed on this continent-wide motion were the subsidence and subsequent uplift of the Eromanga Basin and most of the eastern margin. The Eromanga Basin experienced a rapid pulse of subsidence at 100 Ma, amounting to ~500 m of tectonic subsidence in 10 million years (My) (10). Many of the sediments from the Early Cretaceous were marine and associated with a general marine incursion. The thermal history of sediments inferred from apatite fission track analysis suggests that the Cretaceous section was probably deposited and then eroded in the Surat Basin and the basins on the eastern margin (11). This suggestion is consistent with the tilting up toward the east of marine strata of areas that were at or below sea level during the Cretaceous (8, 11).

The AAD, a segment of the SEIR between 120° and 128°E, south of the Great Australian Bight (GAB), is characterized by rugged ridge flank morphology, bathymetry 800 m deeper than normal, and a series of

closely spaced fracture zones (2) (Fig. 3A). When the subsidence associated with conductive cooling of oceanic lithosphere is subtracted from bathymetry, the residual topography is characterized by a linear north-south-trending depression from the GAB through the AAD (12) to the Antarctic margin (Fig. 3B). In comparison with global residual oceanic topography, the AAD is the most prominent bathymetric anomaly not associated with present-day subduction (13).

Along the SEIR, Sr, Pb, and Nd isotope systematics of basalts reveal that there are two distinct isotopic provinces: one to the west of the AAD, which is characteristic of the Indian Ocean, and one to the east, which is characteristic of the Pacific Ocean (3) (Fig. 3A). The two provinces together are nearly globally encompassing (14). Such an isotopic boundary could be formed by downwelling of material flowing east-west, parallel to the trend of the SEIR, toward the AAD (3). From a limited number of drill holes, it appears that the boundary between the isotopic provinces has migrated toward the west by a few centimeters per year since 50 Ma (15) (Fig. 3A). Furthermore, the large-scale Indian Ocean isotope province (14) could be a remnant of the former Gondwanaland supercontinent because the isotope systematics are consistent with sediment subduction, among other processes, beneath the continental lithosphere (3, 16).

Major element systematics indicate that basalts from the AAD are consistent with lower than normal mantle temperature and lower extent of melting than under normal ridges (17). As expected, the crust within the AAD is thinner (4.2 km) than an adjacent part of the SEIR (7.2 km) (18) (Fig. 3B). Only about half of the 800-m depth anomaly (Fig. 3B) can be accounted for by thinner crust (19). Consequently, there may be comparable contributions to topography from a thinner crust and the dynamic topography arising from a cold mantle anomaly.

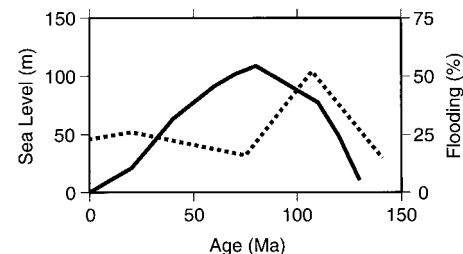


**Fig. 1.** Eustatic sea level (solid line) inferred from passive margins in the Atlantic Ocean (30) and the percentage area of Australia flooded (dotted line) (1).

M. Gurnis is at the Seismological Laboratory, California Institute of Technology, Pasadena, CA 91125, USA. E-mail: gurnis@caltech.edu. R. D. Müller is in the Department of Geology and Geophysics, University of Sydney, Sydney, NSW 2006, Australia. E-mail: dietmar@es.su.oz.au. L. Moresi is at the Australian Geodynamics Cooperative Research Centre, Commonwealth Scientific and Industrial Research Organization Exploration and Mining, Nedlands, WA 6009 Australia. E-mail: louis@ned.dem.csiro.au

## Dynamic Models: Cretaceous to the Present

To explain these two features, we developed a three-dimensional (3D) model of mantle convection with the motions of tectonic plates imposed. Up until the Early Cretaceous, a converging margin between the Pacific plates and Gondwanaland was within a few hundred kilometers of the Australian eastern margin and had existed for the previous 100 My (20). The active margin off eastern Australia ceased at 95 Ma (21). When we fix the Jurassic position of this converging margin in a reference frame fixed with respect to the hot spots (22, 23), we find that this former position of convergence passed under the eastern interior of Australia during the Late Cretaceous and is presently beneath the AAD. The hypothesis that a subducted slab is responsible for the vertical motion and AAD is tested by making comparisons between observed Cretaceous inundation of Australia and present-day geochemical and geophysical observations of the southeast Indian Ocean and dynamic models.

We used a 3D finite element model of thermal convection in a viscously dominated, infinite-Prandtl number fluid, appropriate for flow in Earth's mantle (24). Plate

kinematics, including plate margins, were transformed from a spherical surface to a plane (25). From 130 Ma to the present, plate geometry was imposed as velocity boundary conditions that changed every 10 My.

The initial condition consisted of a slab in its Early Cretaceous position. The Lord Howe Rise (LHR) was rotated back to its priferit position so that our model trench was located parallel to the continental margin (Fig. 4). This model trench is a simplification of the much more extensive Gondwanaland-Pacific margin, where convergence may have extended further toward New Guinea, encompassing West Antarctica and South America (26). Two chemical provinces were created to explore the hypothesis that an initially sharp boundary between two large-scale geochemical provinces, delineated by subduction before Gondwanaland breakup, could be associated with the present boundary observed at the AAD. The two provinces consisted of neutrally buoyant tracers, inserted through the mantle with one group to the west (left) of the slab (Gondwanaland tracers) and the other to the right (east) of the slab (Pacific tracers).

The convection models can be tied to observations by fixing points to plates and

moving those points in time with the imposed plate model. Points fixed to AUS were used as a reference frame for a simple sedimentation model. A synthetic lithosphere was created from the modeled margin between AUS and Antarctica (ANT); from 50 Ma forward, we created oceanic crust with a thickness depending on mantle temperature (27) below the ridge and a trace element chemistry by sampling the tracers. A crustal thickness and composition were assigned to points and subsequently moved according to the plate model. We explored a variety of cases in which we varied parameters associated with uncertainties in the initial configuration of subduction and uncertainties intrinsic to the mantle.

**Plate kinematics and topography.** We considered a nominal model (28) of a 100-Ma, 30° dipping slab in which the trench is on average 1400 km east of the present coastline of Queensland (Fig. 4). In the marginal area off the coast, there was a prominent linear topographic depression (Fig. 5A) that can be associated with an oceanic trench. Initially, the slab was attached to the oceanic lithosphere; if subduction continued, the spatial evolution of volcanism and rifting indicates that it did so further toward the east (20). From 130 Ma to the present, the slab descended under its own weight, and later partially drawn upward under a ridge.

In nearly all cases explored, we noted two consistent features in the topography of the plates directly related to plate motions. During the first phase, there was a general motion toward the Pacific by the three plates making up Gondwanaland (AUS, LHR, and ANT) with velocities exceeding 5 cm/year with respect to the hot spot reference frame (Fig. 5, A to C). During this phase of plate motion, Australia migrated over the topographic depression generated by the slab. From 120 to 110 Ma, the eastern interior of Australia was over the former position of subduction, a downwelling (Fig. 6A) with up to ~350 m of overlying dynamic topography (Fig. 5B). There was continued slow migration of the topographic depression westward through the continent while the amplitude of dynamic topography decayed; since the topography decayed, Australia uplifted by about 200 m from 110 to 60 Ma. The second phase followed a period of relative quiescence (during which time AUS rifted from ANT but moved only slowly northward); Australia started moving away from Antarctica at about 50 Ma with nearly constant velocity between 7 and 8 cm/year. During the second phase, while Australia started in a nearly stationary position over a mild, about

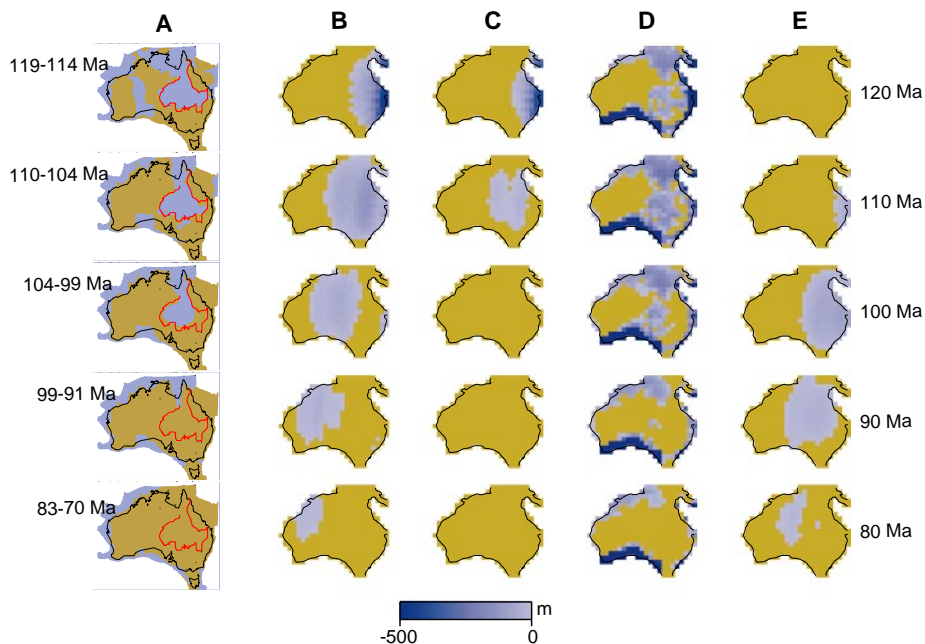


**Fig. 2. (A)** Paleogeographic reconstructions of Australia during the Cretaceous (36); blue shading denotes marine inundation, and brown shading denotes those parts of the continent that are subaerially exposed. The age ranges to the left refer only to the inferred paleogeographic reconstructions. The red outline denotes the Eromanga and Surat basins. **(B to E)** Predicted marine inundation of Australia from convection models. Ages to the right refer only to models. Blue areas are those areas covered by shallow seas; brown shading denotes those parts of the continent predicted to be exposed. **(B)** Nominal case with sedimentation rate of 5 m/My. **(C)** The same as **(A)**, except for 10 m/My. **(D)** The same as **(A)**, except with the initial topography set to present observed values. Accommodation spaces of less than -500 m have been truncated in **(D)**. **(E)** Slab with a 30° dip angle and 2400 km off the Australian margin with 5 m/My.

–100 m, nearly continental-scale topographic depression (Fig. 5D), the SEIR started to spread faster, and a concentrated, nearly circular depression formed at the ridge near the GAB (Fig. 5E). The amplitude of this concentrated depression increased from 45 Ma onward, and its magnitude increased substantially over the past 20 My (Fig. 5F).

During the first phase of eastward motion, the slab (Fig. 4) became partially stalled above the endothermic phase transition (Fig. 6A). From 60 Ma (Fig. 6B) to the present, cold subducted material was drawn upward beneath the ridge (Fig. 6, C to D). Currently, the position of the ridge (R in Fig. 6D) is above the area where mantle, a few tens of degrees cooler than normal, is being drawn upward in our model. The circular topographic depression (Fig. 5F) is caused by a linear source of buoyancy orthogonal to the upwelling flow.

**Integration with sedimentation.** We attempted to predict the marine inundation of Australia. For each point fixed to Australia, sediment accumulates at a constant rate between the sea and solid surfaces, a difference referred to as accommodation space. The sea surface is maintained at a constant height (29) that is equal to the average global sea level (30). The solid surface is originally either a constant height, 150 m, or equal to present topography. Both models are simplifications, but topography within the continental interior, much of which existed in the Cretaceous, is substantial and affects marine inundation (1). We added dynamic topography at 130 Ma, and subsequently the surface height changed as sediment accumulated and topography changed. Basement topography changed for a given point as that point moved with the plate over the evolving dynamic topography. Positive accommodation spaces are those areas predicted to be inundated. For our nominal model with an initially flat surface and a sedimentation rate of 5 m/My (31), the eastern portion of Australia flooded at 120 Ma with a nearly uniform tilt downward toward the east (Fig. 2B), related to the rapid eastward motion of Australia over the slab (Fig. 5, A to B). From 120 to 100 Ma, the inundation broadened westward with decreasing accommodation spaces. By 90 Ma, however, a smaller portion of the west was covered by a thin veneer of sediments such that, by 80 Ma, the continent had been completely exposed, despite the increasing height of global sea level, which peaked at ~70 Ma (Fig. 1). From 80 Ma to the present, the model continent remained completely exposed. By increasing the sedimentation rate from 5 to 10 m/My (Fig. 2C), the marine inundation became more confined to the east, with

earlier exposure of the continent during the sea-level rise. The continent became exposed because with small sedimentation rates and increasing sea level, there was uplift on a continental scale as dynamic topography decayed. Unfortunately, both models had inundation and sediment accumulation in the western half of the platform from 100 to 70 Ma, when no such marine sedimentation occurred. With the use of an initial solid surface equal to the present continental topography and a sedimentation rate of 5 m/My, a more acceptable pattern of inundation (Fig. 2D) and sediment distribution emerged.

**Present-day geophysics and geochemistry.** With this dynamic model, we predict the present-day structure of the oceanic lithosphere between Australia and Antarctica. At present, an abrupt change in chemistry is delineated by the sampled passive tracers (Fig. 3C) just to the left (west) of the dynamic topography depression, at 130°E. Moreover, the boundary between these two provinces has migrated to the west with an apparent velocity of ~3 to 4 cm/year, as a consequence of the eastward component of AUS and ANT motion in the fixed hot spot reference (Fig. 5F). Furthermore, a 300-km-wide region of thinned

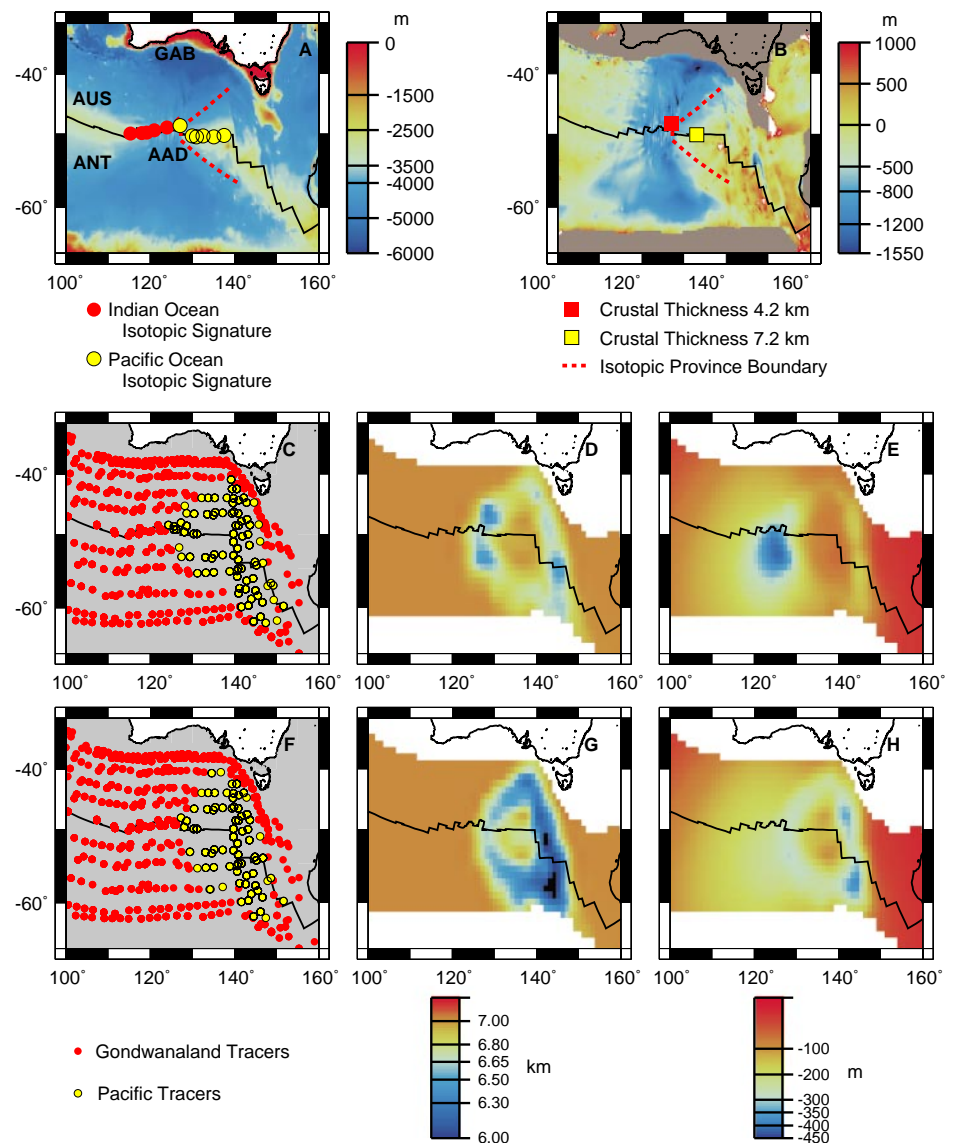


**Fig. 3.** Observed and predicted characteristics of the southeast Indian Ocean. (A) Observed bathymetry, isotopic signature of the mid-ocean ridge basalts (3), and inferred migration of the isotopic boundary (15). (B) Bathymetry corrected for conductive cooling (predicted subsidence is  $2600 + 220 \times \text{age}^{1/2}$  in meters and age is in million years) and for sediment loading (13). (C to E) Predictions from nominal model (28). (C) Tracers sampled at the ridge and rotated to present positions. (D) Inferred crustal thickness based on mantle temperature. (E) Total topography on the top surface driven by viscous flow and crustal thickness. (F to H) Same quantities for an identical model, except with no phase changes. (F), (G), and (H) correspond to (C), (D), and (E), respectively.

oceanic crust develops at the ridge such that the center of thinned crust is essentially aligned with the distinct discontinuity in chemistry (Fig. 3D). The thinned crust does not extend uniformly north-south from the ridge; rather, the thinned crust shows an apparent migration to the west. The creation of thinner crust becomes more pronounced at about 20 Ma, from thicknesses only a few hundred meters less than normal

10 My after rifting to 1 km thinner at the present time. The thinned crust is caused by the upwelling of a fraction of old slab that had partially stagnated in the transition zone beneath the ridge (Fig. 6). The onset of thinner crust corresponds to the time it takes the slab to be drawn up from the transition zone (Fig. 6, B to D) starting at ~45 Ma when rifting between Australia and Antarctica accelerated (Fig. 5, D and

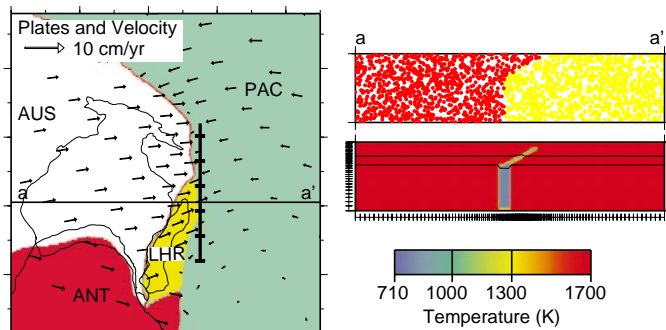
E). Finally at present, dynamic stress and thinner crust give rise to a 500-m topographic depression on the ridge in the vicinity of 125°E (Fig. 3E).

**Influence of mantle rheology and phase transitions.** To explore the sensitivity of results to assumed mantle characteristics, we varied the temperature dependence and radial variation in viscosity and strength of phase transitions at 410- and 660-km depth. With a model that incorporated a temperature-dependent viscosity (32), slab descent diminished to only a few millimeters per year in the upper mantle and stagnated within the lower mantle because the slab could not deform and bend at the bottom boundary—not unlike the stagnation of the top thermal boundary layer in thermal convection with temperature-dependent viscosity (33). Studies of geoid anomalies over slabs also suggest that slabs are weak (24). The magnitude of dynamic topography increased by about 20% compared with the nominal case for all times, but more importantly, the decay of dynamic topography from 120 to 60 Ma and its subsequent re-appearance when Australia and Antarctic separated were not nearly as pronounced with strong as compared with weak slabs.

The effect of the exothermic phase change at 410 km was minor, but that of the phase change and viscosity jump at 660 km was strong. When the viscosity contrast between the upper and lower mantle was held constant and both phase transitions were eliminated, we found that a substantial fraction of the slab could no longer be trapped above 660-km depth for substantial time periods compared with a case with both phase changes present. The trapping of the slab by positive buoyancy of an endothermic phase change at 660 km, especially when the slab had been sheared out by the eastward motion of Gondwanaland from 130 to 90 Ma (for example, Fig. 5, A to C, and Fig. 6A), played a fundamental role in the appearance of a distinct topographic depression and thin crust along an isolated part of the SEIR. This model not only predicted a mild undulation in topography (Fig. 3H) but was unable to reproduce the thinner crust near 130°E, especially the onset of thinner crust at 20 Ma (Fig. 3G).

**Influence of initial conditions.** The sensitivity of model outcomes resulting from uncertainty in Early Cretaceous paleogeography was explored by varying the initial values of the following parameters: the position of the trench, the initial dip angle of the slab, the amount of slab within the lower mantle, and the age of subducting lithosphere. Moving the trench an additional 1000 km from the Australian margin while keeping slab dip constant at 30° delayed the time of inundation such that

**Fig. 4.** (Left) Initial condition for nominal model (28) with plate stencils and imposed velocity vectors. The position of the trench is shown by the vertical line with the crossing tick marks such that the slab extends from  $y = 1.2$  to  $3.2$ . Major tick marks on the box edges have a 2000-km spacing. The domain is Cartesian with horizontal dimensions  $4.5 \times 4.8$



and a depth of 1. All of the models are based on a box depth of 2000 km; this depth is less than that of the whole mantle but has a volume greater than the mantle under an equivalent area of Earth's surface. (Right) The initial configuration of the slab is shown for line a-a'; the center of the slab delineates the initial position of the "Gondwanaland" tracers in red and the "Pacific" tracers in yellow.

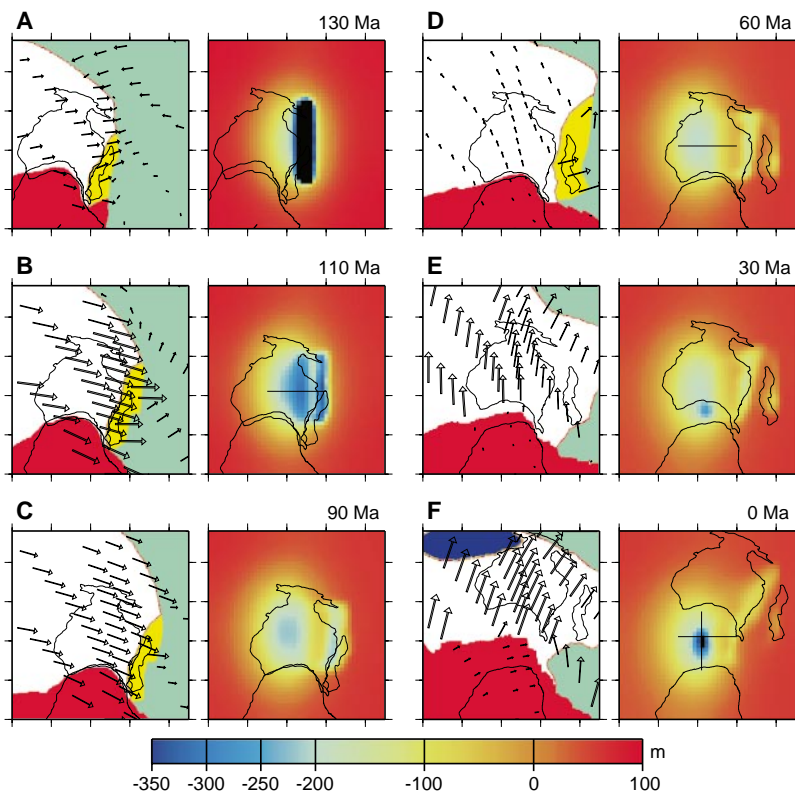


**Fig. 5.** Plate stencils and imposed plate velocity (left) and predicted dynamic topography at six times [(A) 130 Ma, (B) 110 Ma, (C) 90 Ma, (D) 60 Ma, (E) 30 Ma, and (F) 0 Ma] for the nominal model (right) (28). The dynamic topography was computed for a no-slip top boundary condition. The black lines in (B), (D), and (F) denote the temperature cross sections shown in Fig. 6, A to C, respectively. In (A), topography greater than  $-350$  m is shown in black and reaches a maximum value of  $-1200$  m. In (F), the maximum topography is  $-350$  m.

there is no inundation in the eastern half of the platform at 120 to 100 Ma (Fig. 2E), as required by the observed distribution of sediments (Fig. 2A). Moreover, the position of the topographic and geochemical anomaly along the present-day ridge was shifted toward the east in comparison with the nominal model. Decreasing the age of the slab from 100 to 50 Ma had little effect, because with its reduced buoyancy the rate of slab descent decreased, so although the slab weighed less, the buoyancy source was closer to the surface at any time and the net change on the dynamic topography was small. During the final 20 My of the model, when cold material was drawn up by the ridge, fluid in the transition zone was warmer (compared with the case with an older slab) such that it was drawn up more effectively. Without slab extension into the lower mantle, a larger fraction of cold fluid remained in the upper mantle to decrease the temperature beneath the ridge and dynamically pull the topography downward. Crust was thinner and bathymetry deeper with smaller amounts of slabs initially in the lower mantle.

## Discussion

For a range of reasonable values, we are able to match observed inundation of Australia (Fig. 2A) with simple dynamic models of convection with imposed plate tectonics (Fig. 2D). The uplift of Australia is a natural consequence of dynamic topography that decreases with the demise of subduction on the Pacific margin of Australia during the Cretaceous. The most important limitation of the present models is the inability to explain the permanent subsidence of the Eromanga and Surat basins. Qualitatively, about half of the Cretaceous subsidence of these basins was recovered during the Cenozoic, and half persists to the present (8, 11). By itself, dynamic topography is incapable of explaining permanent subsidence of sedimentary basins, because it is reversible. But it is the reversible nature of dynamic topography that allows us to explain the uplift and exposure of the eastern half of the continent, even as global sea level rises.

The same dynamic models are also able to match the present-day geochemistry and geophysics of the SEIR, including the prominent topography on the ridge (Fig. 3E), thin crust at  $\sim 130^\circ\text{E}$  (Fig. 3D), the onset of anomalous tectonics over the past tens of millions of years (Fig. 3D), the sharp jump of an otherwise long wavelength isotopic signature along the ridge (Fig. 3C), and the apparent westward migration of the isotopic anomaly at a few centimeters per year (Fig. 3C). The models show that the intensity of

the dynamic stress (dynamic topography) increased over the past tens of million years, commensurate with the onset of formation of thin oceanic crust, as cold mantle was advected closer to the surface. This result is consistent with the increasing roughness of sea-floor topography and development of fracture zone offsets in the AAD over the Neogene (2).

The primary control on the development of an anomalous ridge structure by an old slab is the presence of an endothermic phase change at 660-km depth along with a jump in effective viscosity between transition zone and lower mantle that tends to trap a flat laying slab before being partially drawn upward by the new spreading center. Results from seismic tomography and dynamic models have shown that trapping of slabs within the transition zone may be a common attribute of subduction dynamics. This trapping is best displayed beneath the Izu Bonin Arc south of Japan, where the slab is flat laying and trapped in the transition zone over a horizontal distance of about 700 km (34), much like the structures displayed by the dynamic models (Fig. 6A). In both the mantle and dynamic models, these flat laying structures are best displayed in converging margins that are actively migrating oceanward (35), probably identical to the tectonics of the Australian eastern

margin during the Cretaceous (20, 21).

The model we are proposing for the formation of the AAD is different from other models based on isotope geochemistry (4); in these models, the source of the AAD is actively moving toward the west and driven by mantle flow from the Pacific to Indian oceans. During the opening of the SEIR, the trapped portion of the slab within the transition zone moves little horizontally, and the apparent migration is primarily due to the motion of the plates toward the east in the hot spot frame. Consequently, the AAD is much like a track of a hot spot, except that here we are dealing with the track of a cold spot.

Individually, the correspondence between a predicted and an observed quantity is not perfect—the importance of our results is the ability to predict the wide suite of disparate observations. These observations include the subsidence and uplift of Australia during the Cretaceous; the westward migration of an isotopic boundary in the ocean basin; a distinct crustal thickness, isotopic structure, and topographic structure at the approximate position of the present AAD; and the disruption of the oceanic crust since the start of the Neogene. By following the evolution of the global ridge system with respect to long-lived Mesozoic subduction in a hot spot reference frame (22, 23, 25), we find that the SEIR was the only ridge to override an old subduction zone. This overriding is probably the reason why the AAD is a unique feature of the global system of ridges. We have not attempted to adjust mantle or paleogeographic parameters to improve the fit with observed quantities. Clearly, there are substantial opportunities to adjust parameters, and in fact we believe that by finding the best match with observations, fundamental constraints can be placed on mantle and slab rheology and the Mesozoic paleogeography of the Gondwanaland-Pacific margin.

## REFERENCES AND NOTES

1. J. J. Veevers, Ed., *Phanerozoic Earth History of Australia* (Clarendon, Oxford, 1984), pp. 210–221.
2. J. K. Weissel and D. E. Hays, *J. Geophys. Res.* **79**, 2579 (1974).
3. E. M. Klein, C. H. Langmuir, A. Zindler, H. Staudigel, B. Hamelin, *Nature* **333**, 623 (1988).
4. B. P. West, W. S. D. Wilcock, J.-C. Sempere, L. Geli, *J. Geophys. Res.* **102**, 7783 (1997).
5. J. J. Veevers, *Nature* **295**, 315 (1982).
6. H. I. M. Struckmeyer and P. J. Brown, *BMR Record 1990/11* (Bureau of Mineral Resources, Canberra, Australia, 1990).
7. G. Bond, *Geology* **6**, 247 (1978).
8. M. Russell and M. Gurnis, *Basin Res.* **6**, 63 (1994).
9. The Eromanga and Surat basins form an extensive intracratonic basin system containing up to 3.5 km of Cretaceous and Jurassic sediments and occupying a combined area of  $1.5 \times 10^6 \text{ km}^2$  [N. F. Exon and B. R. Senior, *BMR J. Aust. Geol. Geophys.* **1**, 33 (1976)].

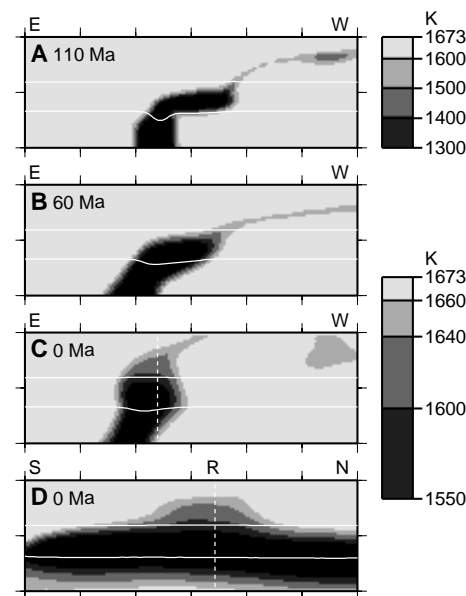


**Fig. 6.** Vertical cross sections of temperature for nominal model (28). (A to C) Nearly east-west profiles. (D) A south-north section orthogonal to (C) with respective lines of intersection shown by white dashed vertical lines. Locations of cross sections are shown as black lines in Fig. 5, B, D, and F. The upper scale is for (A) only (representing a large temperature span), and the lower scale is for (B) to (D). R denotes the position of the ridge. The tick marks have a 500-km spacing.

10. K. Gallagher and K. Lambeck, *Basin Res.* **2**, 115 (1989).
11. K. Gallagher, T. A. Dumitru, A. J. W. Gleadow, *ibid.* **6**, 77 (1994).
12. J. R. Cochran and M. Talwani, *Geophys. J. R. Astron. Soc.* **50**, 495 (1977).
13. F. Pribac, thesis, Australian National University, Canberra (1991).
14. S. R. Hart, *Nature* **309**, 753 (1984).
15. D. G. Pyle, D. M. Christie, J. J. Mahoney, R. A. Duncan, *J. Geophys. Res.* **100**, 22261 (1995).
16. D. G. Pyle, D. M. Christie, J. J. Mahoney, *Earth Planet. Sci. Lett.* **112**, 161 (1992); M. Rehkämper and A. W. Hofmann, *ibid.* **147**, 93 (1997).
17. E. M. Klein and C. H. Langmuir, *J. Geophys. Res.* **92**, 8089 (1987).
18. M. Tolstoy, A. J. Harding, J. A. Orcutt, J. Phipps Morgan, *Eos (Fall Suppl.)* **76**, 570 (1995).
19. Using the observed difference in crustal thickness (78) and a simple isostatic balance ( $\rho_c = 2900 \text{ kg/m}^3$  and  $\rho_m = 3250 \text{ kg/m}^3$ ), we predicted a bathymetric difference of 470 m, smaller than the observed ~750 m. Using a more sophisticated isostatic balance and observed major element chemistry, P. Lecroart, A. Cazenave, Y. Ricard, C. Thoraval, and D. G. Pyle [*Earth Planet. Sci. Lett.* **149**, 49 (1997)] have predicted a 400-m difference between observed and isostatic topography.
20. Subduction off eastern Australia was but a part of the larger Pacific-Gondwanaland converging margin [B. C. Storey, *Nature* **377**, 301 (1995)]. The early Mesozoic margin, which included New Caledonia, New Zealand, Lord Howe Rise, and Norfolk ridge, was typified by convergence and calc-alkaline volcanism that progressively migrated outboard as the style of the Australian margin shifted to rifting in the Cretaceous, as summarized by N. Williams and R. Korsch [in *Extended Abstracts 43* (Geological Society of Australia, Sydney, 1996), pp. 564–568].
21. The Whitsunday volcanic province represents the tail end of rifting in a back arc setting [S. Bryan, in *Extended Abstracts 43* (Geological Society of Australia, Sydney, 1996), pp. 124–133].
22. The reconstructions were based on the hot spot reference frame of R. D. Müller, J.-Y. Royer, and L. A. Lawver [*Geology* **21**, 275 (1993)].
23. The Gondwanaland converging margin did not undergo a substantial shift in paleolatitude from ~200 to ~120 Ma, as seen in paleogeographic reconstructions [L. A. Lawver and L. M. Gahagan, in *Flow and Creep in the Solar System*, D. B. Stone and S. K. Runcorn, Eds. (Kluwer Academic, Dordrecht, Netherlands, 1993), pp. 225–247].
24. L. Moresi and M. Gurnis, *Earth Planet. Sci. Lett.* **138**, 15 (1996).
25. The continental outlines, isochrons, and referenced rotation poles of R. D. Müller, U. R. Roest, J.-Y. Royer, L. M. Gahagan, and J. G. Scialer [*J. Geophys. Res.* **102**, 3211 (1997)] were used and transformed to a Cartesian domain with an azimuthal Lambert equal area projection.
26. Our models showed that slabs, while in the lower mantle, only moved laterally by about 500 km, and consequently our focus on a segment of the margin confined to beneath Australia and the SEIR was justified.
27. Thermodynamic calculations and petrologic models estimate that oceanic crustal thickness increases 0.06 km for each 1°C increase in mantle temperature [C. H. Langmuir, E. M. Klein, T. Plank, in *Mantle Flow and Melt Generation*, J. Phipps Morgan, Ed. (American Geophysical Union, Washington, DC, 1992), pp. 183–280; P. Asimow, thesis, California Institute of Technology, Pasadena (1997)]. Crustal thickness is computed by sampling the temperature within a 200-km region beneath the ridge.
28. The nominal model had a Rayleigh number of  $7.4 \times 10^6$  (based on upper mantle and transition zone viscosity of  $10^{21}$  Pa-s), no temperature-dependent viscosity, and a 100-fold jump in viscosity at 660 km. The Clapeyron slope and jump in density were 2.0 MPa/K and 5% at 410 km and -4.2 MPa/K and 8% at 660 km. The upper 100 km was assumed to be lithosphere, with a viscosity 100 times that of the upper mantle.
29. Geoid height variations are ignored because its amplitude is smaller than the dynamic topography, such that topography is the primary dynamic control on sea-level change [M. Gurnis, *Nature* **344**, 754 (1990); C. Lithgow-Bertelloni and M. Gurnis, *Geology* **25**, 735 (1997)].
30. A. B. Watts and M. S. Steckler, in *Deep Drilling Results in the Atlantic Ocean: Continental Margins and Paleoenvironments*, M. Talwani, W. Hays, W. B. F. Ryan, Eds. (American Geophysical Union, Washington, DC, 1979), pp. 218–234.
31. L. L. Sloss, in *Sedimentary Cover—North American Craton: U.S.*, L. L. Sloss, Ed. (Geological Society of America, Boulder, CO, 1988), pp. 25–51.
32. For temperature-dependent viscosity, an Arrhenius form with an activation energy of 400 kJ/mol with a 100-fold truncation in lateral variation was used.
33. U. Christensen, *Geophys. J. R. Astron. Soc.* **77**, 343 (1984).
34. R. van der Hilst and T. Seno, *Earth Planet. Sci. Lett.* **120**, 395 (1993).
35. R. van der Hilst, *Nature* **374**, 154 (1995); S. Zhong and M. Gurnis, *Earth Interact.* [online] **1** (no. 6) (1997), available at <http://earthinteractions.org>.
36. BMR Paleogeographic Group, *Cretaceous Paleogeographic Maps Record 1990/30 Paleogeographic Series 14* (Bureau of Mineral Resources, Canberra, Australia, 1990).
37. This report represents contribution 8489 of the Division of Geological and Planetary Sciences, California Institute of Technology. Some of the work reported here was conducted as part of the Australian Geodynamics Cooperative Research Centre (AGCRC) and is published with the consent of the Director, AGCRC. We thank J. Veevers for taking the time to discuss the geologic constraints on Mesozoic subduction beneath Australia and K. Gallagher and J. Veevers for helpful comments on the manuscript.

3 November 1997; accepted 28 January 1998

# Crystal Structures of Human Topoisomerase I in Covalent and Noncovalent Complexes with DNA

Matthew R. Redinbo,\* Lance Stewart,\*† Peter Kuhn, James J. Champoux, Wim G. J. Hol‡

Topoisomerases I promote the relaxation of DNA superhelical tension by introducing a transient single-stranded break in duplex DNA and are vital for the processes of replication, transcription, and recombination. The crystal structures at 2.1 and 2.5 angstrom resolution of reconstituted human topoisomerase I comprising the core and carboxyl-terminal domains in covalent and noncovalent complexes with 22–base pair DNA duplexes reveal an enzyme that “clamps” around essentially B-form DNA. The core domain and the first eight residues of the carboxyl-terminal domain of the enzyme, including the active-site nucleophile tyrosine-723, share significant structural similarity with the bacteriophage family of DNA integrases. A binding mode for the anticancer drug camptothecin is proposed on the basis of chemical and biochemical information combined with these three-dimensional structures of topoisomerase I–DNA complexes.

Topoisomerases are ubiquitous enzymes that solve topological problems generated by key nuclear processes such as DNA replication, transcription, recombination, repair, chromatin assembly, and chromosome segregation (1). There are two types of topoisomerases. Type I enzymes are monomeric and transiently break one strand of duplex DNA, allowing for single-step changes in the linking number of circular DNAs (the number of times one strand of DNA crosses the other). Type II enzymes are dimeric and break both strands of a duplex to generate a gate through which another region of DNA can be passed, resulting in linking number changes in steps of two. Type I and type II enzymes are fundamentally different in both mechanism and cellular function (2–4). The medical importance of these enzymes is underscored by the fact that they are the specific targets of many promising anticancer drugs (5).

Eukaryotic type I topoisomerases differ significantly from their prokaryotic counterparts. Prokaryotic enzymes require magnesium and a single-stranded segment of DNA; additionally, they form a covalent intermediate with the 5′ end of the broken DNA strand and relax only negatively supercoiled DNA. Eukaryotic topoisomerase I enzymes, in contrast, do not require any metal cofactor, need no single-stranded stretch of DNA, form a covalent intermediate with the 3′ end of the broken strand, and are able to relax both positive and negative supercoils. All available evidence indicates that prokaryotic and eukaryotic type I enzymes share no sequence or structural similarity. Vaccinia virus topoisomerase (6), however, shares several mechanistic and sequence features with eukaryotic type I topoisomerases but is much smaller (36 kD) than all known cellular topoisomerases I (7), which range from 80 to 110 kD (8). So far, no structure of a eukaryotic topo-